НАУЧНО-ТЕХНИЧЕСКИЙ ВЕСТНИК ИНФОРМАЦИОННЫХ ТЕХНОЛОГИЙ, МЕХАНИКИ И ОПТИКИ
сентябрь–октябрь 2026 Том 26 № 5 http://ntv.ifmo.ru/
SCIENTIFIC AND TECHNICAL JOURNAL OF INFORMATION TECHNOLOGIES, MECHANICS AND OPTICS
September–October 2026 Vol. 26 No 5 http://ntv.ifmo.ru/en/
ISSN 2226-1494 (print) ISSN 2500-0373 (online)

doi: 10.17586/2226-1494-2026-26-5-1057-1064

Operability of a low-temperature rectification scheme under variations in associated petroleum gas composition

Vadim O. Kholyavkin[1]✉, Ekaterina V. Logvinenko[2]

[1,2] ITMO University, Saint Petersburg, 197101, Russian Federation

[1] vadimixl@itmo.ru✉, https://orcid.org/0009-0006-3263-822X
[2] evlogvinenko@itmo.ru, https://orcid.org/0000-0002-2155-2109

Abstract

The composition of Associated Petroleum Gas (APG) varies between fields and during field development, which affects phase behavior and component distribution in Low-Temperature Rectification (LTR) units. Because industrial pressure and temperature set-points are fixed or adjustable only within narrow limits, the relevant task is to determine whether an existing scheme remains operable without retuning when feed composition changes. A steady-state Aspen HYSYS model was developed for a mixture containing CH_4, C_2H_6, C_3H_8, i-C_4H_{10}, n-C_4H_{10}, and a lumped C_{5+} fraction. Five reference APG compositions were simulated at identical set-points. For each component i, recovery to the bottoms, R_i, was calculated as the component mass flow in the bottoms divided by its total mass flow in the overhead and bottoms products. Recoveries for 100 realistic compositions were estimated by inverse-distance weighting in composition space. A case was classified as operable when methane recovery to the bottoms did not exceed 0.05, propane recovery was at least 0.905, and recoveries of i-butane, n-butane, and C_{5+} were at least 0.95. Under the selected fixed set-points, 85 of 100 compositions met all criteria, giving an operability index $F = 0.85$. The PASS/FAIL map showed that propane recovery is the limiting criterion near the operability boundary, whereas butanes and C_{5+} retain larger margins. The proposed method identifies the feed-composition domain in which an LTR scheme remains operable at fixed set-points while reducing the number of full process simulations. Its validity is limited to the composition domain covered by the reference cases; therefore, borderline and extrapolative cases require targeted simulations.

Keywords

associated petroleum gas, low-temperature rectification, scheme operability, feed-composition variation, component recovery, inverse-distance weighting, Aspen HYSYS, feasibility map

For citation: Kholyavkin V.O., Logvinenko E.V. Operability of a low-temperature rectification scheme under variations in associated petroleum gas composition. *Scientific and Technical Journal of Information Technologies, Mechanics and Optics*, 2026, vol. 26, no. 5, pp. 1057–1064. doi: 10.17586/2226-1494-2026-26-5-1057-1064

УДК 665.612.2:66.048.3

Оценка работоспособности схемы низкотемпературной ректификации при изменении состава попутного нефтяного газа

Вадим Олегович Холявкин[1]✉, Екатерина Владимировна Логвиненко[2]

[1,2] Университет ИТМО, Санкт-Петербург, 197101, Российская Федерация

[1] vadimixl@itmo.ru✉, https://orcid.org/0009-0006-3263-822X
[2] evlogvinenko@itmo.ru, https://orcid.org/0000-0002-2155-2109

Аннотация

Введение. Состав попутного нефтяного газа изменяется как между месторождениями, так и по мере их разработки, что влияет на фазовое состояние потоков и распределение компонентов в установках низкотемпературной ректификации. Поскольку промышленные уставки давления и температуры фиксированы или регулируются в ограниченных пределах, практической задачей является оценка работоспособности существующей схемы без перенастройки режима при изменении состава сырья. **Метод.** В составе программного пакета «Aspen HYSYS» разработана стационарная модель для смесей CH_4, C_2H_6, C_3H_8, i-C_4H_{10}, n-C_4H_{10} и

© Kholyavkin V.O., Logvinenko E.V., 2026

укрупненной фракции C_{5+}. Пять опорных составов попутного нефтяного газа рассчитаны при одинаковых уставках. Для каждого компонента *i* степень извлечения в кубовый продукт R_i определена как отношение массового расхода компонента в кубовом продукте к его суммарному расходу в верхнем и кубовом продуктах. Значения извлечения для 100 реалистичных составов оценены методом обратных расстояний в пространстве состава. **Основные результаты.** Схема считалась работоспособной, если извлечение метана в кубовый продукт не превышало 0,05, извлечение пропана — не менее 0,905, а извлечение i-бутана, n-бутана и фракции C_{5+} — не менее 0,95. При выбранных фиксированных уставках всем критериям соответствовали 85 из 100 составов, что дало индекс работоспособности $F = 0,85$. Карта PASS/FAIL показала, что вблизи границы работоспособности лимитирующим критерием является извлечение пропана, тогда как для бутанов и фракции C_{5+} сохраняется больший запас. **Обсуждение.** Предложенный метод позволяет определить область составов сырья, в которой схема низкотемпературной ректификации сохраняет работоспособность при фиксированных уставках, и дает возможность сократить число полных имитационных расчетов. Метод применим в пределах области, охваченной опорными составами; пограничные случаи и экстраполяция требуют проверочных расчетов.

Ключевые слова

попутный нефтяной газ, низкотемпературная ректификация, работоспособность схемы, изменение состава сырья, извлечение компонентов, метод обратных расстояний, Aspen HYSYS, карта работоспособности

Ссылка для цитирования: Холявкин В.О., Логвиненко Е.В. Оценка работоспособности схемы низкотемпературной ректификации при изменении состава попутного нефтяного газа // Научно-технический вестник информационных технологий, механики и оптики. 2026. Т. 26, № 5. С. 1057–1064 (на англ. яз.). doi: 10.17586/2226-1494-2026-26-5-1057-1064

Introduction

Low-Temperature Rectification (LTR) schemes for Associated Petroleum Gas (APG) processing are of practical interest because they allow recovering valuable C_{3+} components and obtaining a methane-rich overhead gas suitable for further use in an integrated gas-processing chain [1–4]. The term C_{3+} refers to propane and all heavier hydrocarbons. In the broader context of APG utilization, these technologies are considered as one of the rational alternatives to flaring since they allow hydrocarbon resources to be converted into marketable gas and liquid products rather than being lost as emissions [5–12]. At the same time, the performance of low-temperature hydrocarbon recovery systems is strongly dependent on feed composition, process configuration, and selected operating conditions [2–4, 13–15].

In industrial practice, however, the APG composition is not constant. It may vary both from field to field and over time during field development, as the ratios between methane, ethane, propane, butanes, and heavier hydrocarbons change [13–15]. For low-temperature separation processes, such variability is especially important because feed composition directly affects phase equilibrium, the degree of pre-condensation, vapor-liquid distribution before separation, and, consequently, the recovery of target components in the rectification section [3, 4, 14–16]. As a result, a process scheme that performs satisfactorily for one APG composition may exhibit different separation behavior when the feed becomes lighter or heavier.

LTR units are usually operated under constraints imposed by equipment design and established operating practice. Pressure levels, target temperatures after key heat-exchange stages, and the thermal state of the top section are typically fixed or can only be adjusted within a limited range. Therefore, in real operation, continuous re-optimization of the regime for each new feed composition is impractical. Under such conditions, the most relevant question is not the maximum achievable recovery under newly optimized set-points, but the operability of the existing scheme at fixed operating conditions when feed composition changes. From a technological standpoint, this issue is directly related to whether the scheme continues to provide the required methane rejection to the overhead product and sufficient recovery of C_{3+} components to the bottoms product.

A considerable number of studies have addressed the assessment and optimization of Natural Gas Liquids recovery processes, including turboexpander-based systems, cryogenic separation schemes, and intensified downstream hydrocarbon processing [1–4]. These works demonstrate the importance of process selection and show that recovery efficiency may vary significantly with feed properties and operating parameters. Nevertheless, the main emphasis in the literature is usually placed either on comparing alternative technologies or on finding optimal conditions for a given feed composition [1–3]. Such an approach is useful at the design stage, but it does not fully resolve the applied problem of determining whether an already selected LTR scheme remains operable over a realistic range of APG compositions without repeated tuning of set-points.

For this reason, the present study considers APG composition variability as the main disturbing factor and evaluates the operability of a given LTR scheme under unchanged operating conditions. In this work, operability is understood as the ability of the scheme to ensure the required distribution of key components between the overhead and bottoms products for a realistic set of feed compositions. To address this task, a steady-state model of the process was developed in Aspen HYSYS which is widely used for hydrocarbon-process simulation and engineering analysis [17, 18]. Instead of performing a large number of full simulations for all possible feed compositions, the study combines a limited number of reference calculations with interpolation in composition space. This allows estimating the admissible operating region, identifying limiting compositions, and quantifying the share of feed cases for which the scheme remains operable at fixed set-points.

Thus, the aim of this study is to assess the operability of an LTR scheme under changes in APG composition at fixed

operating conditions and to identify the component group that becomes limiting near the boundary of admissible operation.

System under study and source data

The system under study is an industrial LTR scheme for APG. It comprises recuperative feed cooling, vapor–liquid separation, turboexpansion and Joule–Thomson throttling for cold generation, a rectification column, and bottoms stabilization. The analysis is restricted to steady-state operation at fixed pressure, temperature, and flow-rate set-points; therefore, differences between cases are attributable solely to feed composition.

The feed is represented as a hydrocarbon mixture within the CH_4–C_{5+} system without non-hydrocarbon impurities. This assumption isolates the effect of hydrocarbon composition on methane rejection and C_{3+} recovery. The model includes CH_4, C_2H_6, C_3H_8, i-C_4H_{10}, n-C_4H_{10}, and a lumped C_{5+} fraction. The C_{5+} fraction represents the combined content of pentane and all heavier hydrocarbons.

Vapor–liquid equilibria and thermophysical properties are calculated using the Peng–Robinson equation of state with standard binary interaction parameters. The same convergence tolerances and material- and energy-balance criteria are used in all simulations.

Five reference feeds (A–E) were selected from operational APG compositions after conversion to a common mass-fraction basis and normalization. The set represents a lean composition, a typical composition, and compositions enriched in propane, butanes, and heavier hydrocarbons. Each reference feed was simulated at identical set-points, and the resulting component recoveries to the bottoms were used as reference process responses.

A further set of 100 realistic CH_4–C_{5+} compositions was generated within the observed operating ranges. The propane, i-butane, n-butane, and C_{5+} fractions were varied independently within practical bounds, while methane closed the material balance. All compositions were checked for normalization, non-negative fractions, and physically plausible heavy-component totals.

The source data therefore consists of the component recoveries obtained for the five reference simulations and the coordinates of the 100 generated feed compositions. These data are used in the interpolation and PASS/FAIL classification described below in Methodology.

All conclusions apply only to the selected fixed set-points, including feed and column pressures, target temperatures after the principal heat exchangers and dephlegmator, and the adopted internal circulation rate.

For the reference simulations, material and energy balances, phase states, and column temperature and composition profiles were checked. For the generated compositions, normalization and range checks were performed before interpolation.

Thus, the data structure separates the influence of feed composition from that of process retuning and provides a reproducible basis for estimating the operability domain.

Methodology

The method transfers the plant "portraits", obtained for five reference feeds, to a set of one hundred realistic compositions at unchanged set-points. For each reference, the process model yields per-component shares in the overhead $F_i^{\uparrow}$ and bottoms product $F_i^{\downarrow}$ streams, where $i \in \{CH_4; C_2H_6; C_3H_8; \text{i-}C_4H_{10}; \text{n-}C_4H_{10}; C_{5+}\}$. The recovery of component i to the bottoms is defined unambiguously as

$$R_i = \frac{F_i^{\downarrow}}{F_i^{\downarrow} + F_i^{\uparrow}},$$

where R_i is recovery of component i to the bottoms product; i is index of a hydrocarbon component; $F_i^{\downarrow}$ is mass flow rate of component i in the bottoms product; $F_i^{\uparrow}$ is mass flow rate of component i in the overhead product.

The vector $\mathbf{R}^{(k)}$ is interpreted as the plant "portrait" at reference point $k \in \{A, B, C, D, E\}$:

$$\mathbf{R}^{(k)} = (R_{CH_4}, R_{C_2H_6}, R_{C_3H_8}, R_{\text{i-}C_4H_{10}}, R_{\text{n-}C_4H_{10}}, R_{C_{5+}})^{(k)},$$

where $\mathbf{R}^{(k)}$ is vector of component recoveries obtained for reference feed composition k; k is index of a reference feed composition, where $k \in \{A, B, C, D, E\}$; $R_i^{(k)}$ is recovery of component i obtained for reference feed composition k.

The composition space is parameterized by the heavy groups

$$\mathbf{x} = (x_{C_3H_8}; x_{\text{i-}C_4H_{10}}; x_{\text{n-}C_4H_{10}}; x_{C_{5+}}), x_j \in [0, 1], \sum_j x_j \le 1,$$

where $\mathbf{x}$ is vector representing a feed composition in the selected composition space; j is index of a coordinate in the feed-composition vector; x_j is mass fraction corresponding to coordinate j of the composition vector.

The methane mass fraction, x_{CH_4}, is not included as an independent coordinate of the composition vector and is determined from the normalization condition as

$$x_{CH_4} = 1 - \sum_{j \in \{x_{C_3H_8}; x_{\text{i-}C_4H_{10}}; x_{\text{n-}C_4H_{10}}; x_{C_{5+}}\}} x_j.$$

The five references are assigned corresponding coordinates $\mathbf{x}^{(k)}$. The flexibility assessment uses a set of generated compositions $\{\mathbf{x}_n\}_{n=1}^{N}$ with total number of generated feed compositions used for the operability assessment $N = 100$, each $\mathbf{x}_n$ normalized and confined to observed operating ranges. $\mathbf{x}_n$ is composition vector of generated feed case n.

Predicted recoveries at an arbitrary composition $\mathbf{x}$ from $\{\mathbf{x}_n\}$ are obtained via local Inverse-Distance Weighting (IDW) in Euclidean metric. Distances to the references are

$$d_k(\mathbf{x}) = \|\mathbf{x} - \mathbf{x}^{(k)}\|_2 = \sqrt{\sum j(x_j - x_j^{(k)})^2},$$

where $d_k(\mathbf{x})$ is Euclidean distance between composition $\mathbf{x}$ and reference composition $\mathbf{x}^{(k)}$; $\mathbf{x}^{(k)}$ is composition vector of reference feed k; $x_j^{(k)}$ is value of coordinate j for reference feed composition k.

Then the set of nearest references $\mathcal{N}_K(\mathbf{x})$ is selected (here $K = 3$). Weights follow a power kernel

$$\omega_k(\mathbf{x}) = \frac{d_k(\mathbf{x})^{-p}}{\sum\limits_{j\in\mathcal{N}_K(\mathbf{x})} d_j(\mathbf{x})^{-p}},\ p = 2,$$

where $\omega_k(\mathbf{x})$ is normalized interpolation weight assigned to reference composition k; $\mathcal{N}_K(\mathbf{x})$ is set of the K reference compositions nearest to composition $\mathbf{x}$; K is number of nearest reference compositions used for local interpolation; p is power parameter of the inverse-distance weighting kernel.

The predicted recoveries are a convex combination of reference portraits:

$$\hat{R}_i(\mathbf{x}) = \sum_{k\in\mathcal{N}_K(\mathbf{x})} \omega_k(\mathbf{x}) R_i^{(k)},$$
$$i \in \{CH_4;\ C_3H_8;\ i\text{-}C_4H_{10};\ n\text{-}C_4H_{10};\ C_{5+}\},$$

where $\hat{R}_i(\mathbf{x})$ is recovery of component i predicted for feed composition $\mathbf{x}$.

If for some k we have $d_k(\mathbf{x}) = 0$ (exact match to a reference), we set $\hat{\mathbf{R}}(\mathbf{x}) = \mathbf{R}^{(k)}$. In case of tied distances, weights are averaged. Before computing ω_k, we verify normalization $\sum\limits_j x_j$ and bounds $x_j \in [0, 1]$.

Qualification against the Introduction criteria is performed by testing a system of inequalities for $\hat{R}_i(\mathbf{x}_n)$. For brevity, define the binary acceptance indicator for generated composition $\mathbf{x}_n$:

$$\mathrm{PASS}(\mathbf{x}_n) = \{\hat{R}_{CH_4}(\mathbf{x}_n) \le 0.05,\ \hat{R}_{C_3H_8}(\mathbf{x}_n) \ge 0.905,$$
$$\hat{R}_{i\text{-}C_4H_{10}}(\mathbf{x}_n) \ge 0.95,\ \hat{R}_{n\text{-}C_4H_{10}}(\mathbf{x}_n) \ge 0.95,\ \hat{R}_{C_{5+}}(\mathbf{x}_n) \ge 0.95\},$$

and the flexibility metric as the share of passing cases

$$F = \frac{1}{N}\sum_{n=1}^{N} \mathrm{PASS}(\mathbf{x}_n),\ N = 100,$$

where F is operability index defined as the fraction of generated feed compositions satisfying all acceptance criteria.

For diagnostics, componentwise margins to the thresholds are computed

$$\Delta_{CH_4}(\mathbf{x}) = 0.05 - \hat{R}_{CH_4}(\mathbf{x});$$
$$\Delta_{C_3H_8}(\mathbf{x}) = \hat{R}_{C_3H_8}(\mathbf{x}) - 0.905;$$
$$\Delta_{i\text{-}C_4H_{10}}(\mathbf{x}) = \hat{R}_{i\text{-}C_4H_{10}}(\mathbf{x}) - 0.95;$$
$$\Delta_{n\text{-}C_4H_{10}}(\mathbf{x}) = \hat{R}_{n\text{-}C_4H_{10}}(\mathbf{x}) - 0.95;$$
$$\Delta_{C_{5+}}(\mathbf{x}) = \hat{R}_{C_{5+}}(\mathbf{x}) - 0.95.$$

Here, Δ_i is the signed margin between the predicted recovery of component i and its acceptance threshold. A positive value indicates compliance with the criterion, whereas a negative value indicates its violation.

The minimum margin is

$$\Delta_{\min}(\mathbf{x}) = \min\{\Delta_{CH_4}(\mathbf{x});\ \Delta_{C_3H_8}(\mathbf{x});\ \Delta_{i\text{-}C_4H_{10}}(\mathbf{x});$$
$$\Delta_{n\text{-}C_4H_{10}}(\mathbf{x});\ \Delta_{C_{5+}}(\mathbf{x})\}.$$

The minimum margin $\Delta_{\min}$ is used to identify borderline cases. Among PASS cases, points with the smallest positive $\Delta_{\min}$ are selected; among FAIL cases, points with $\Delta_{\min}$ closest to zero are selected. These compositions are then re-simulated at the same set-points for spot validation. Agreement is assessed using parity plots, mean absolute error, root mean square error, mean bias, and PASS/FAIL class agreement.

For visualization, a feasibility map is built in the plane ($x_{C_3H_8}$, $x_{i\text{-}C_4H_{10}} + x_{n\text{-}C_4H_{10}}$) for $\{\mathbf{x}_n\}$; marker type encodes PASS/FAIL, and marker size reflects $x_{C_{5+}}$. This projection visually delineates the "operating window" at fixed set-points and highlights regions limited primarily by $\hat{R}_{C_3H_8}$. The approach is a local approximation: validity holds within the region covered by the reference set $\{\mathbf{x}^{(k)}\}$. If regime switching is detected within that region, an additional reference should be added and the interpolation repeated. All conclusions are conditional on the set-points specified in the problem statement, ensuring a clean separation between the effects of variable feed composition and those of retuning the scheme.

Process Technology Description

The process flow diagram of the LTR unit is shown in Fig. 1. The APG feed enters the LTR unit at 9.0 MPa and 10 °C. These inlet conditions provide a common basis for comparing different compositions without changing the operating set-points.

In heat exchanger E-1, the feed is recuperatively cooled by the outgoing product streams to approximately –30 °C. The resulting degree of condensation depends on feed composition and determines the vapor–liquid split upstream of the cold section.

Downstream of E-1, the stream is distributed between separator D-1 and heat exchanger E-2. Vapor separated in D-1 is directed to turboexpander X-1, whereas the liquid is additionally cooled and throttled. This arrangement allocates the available cold between expansion and throttling branches.

The D-1 vapor expands in X-1 to the column pressure of 3.0 MPa and cools to approximately –85 °C. Expansion simultaneously generates refrigeration and shaft power, which may be recovered in a coupled compressor.

The liquid and bypass streams are cooled in E-2 and throttled through VLV-1 and VLV-2 to 3.0 MPa. The resulting two-phase streams, at approximately –65°C, enter the designated feed stages of column T-1.

Rectification occurs in column T-1. The overhead product is an ethane-containing dry gas dominated by CH_4 and C_2H_6 with a low C_{3+} content. The bottoms product is a C_{3+} hydrocarbon concentrate, primarily a propane–butane mixture containing a minor C_{5+} fraction and no more than 5 wt% light components. A side draw of 2,000 kg/h from the fifth theoretical stage is circulated through E-2 to stabilize the cold-end heat balance.

The CH_4–C_2H_6-rich overhead stream is routed through E-1 and provides the main recuperative cooling duty for the incoming APG. After warming, it leaves the heat-exchange network for further treatment or delivery.

Pressure, temperature, level, and flow controllers maintain the principal operating variables. The column pressure is controlled at 3.0 MPa, while the post-dephlegmator temperature determines the upper-section vapor-to-liquid ratio and therefore affects propane retention.

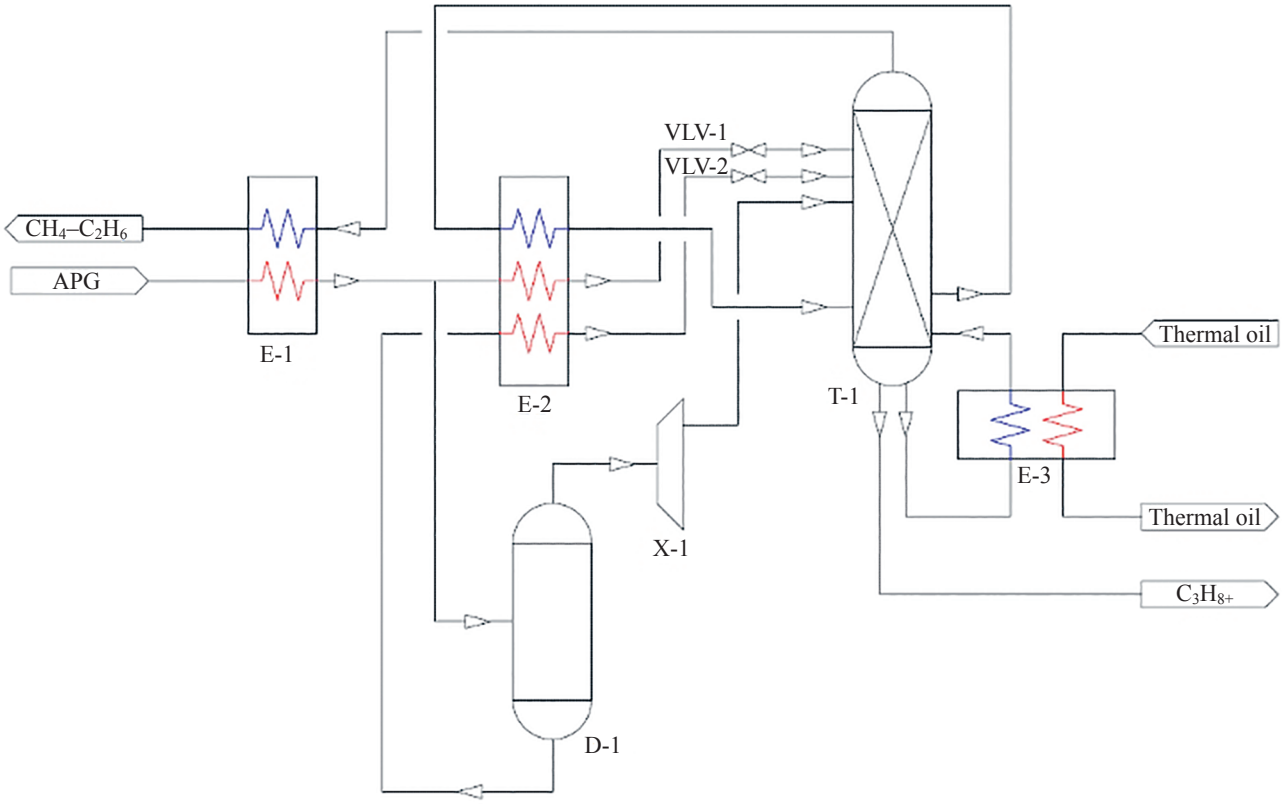

Fig. 1. LTR process flow diagram (red and blue lines indicate the hot and cold heat-transfer streams, respectively)

The process therefore produces an ethane-containing dry gas overhead and a propane–butane-rich liquid bottoms product without an external refrigeration cycle.

The following section quantifies component distribution at the fixed set-points, constructs the PASS/FAIL map, and evaluates the aggregate operability index F.

Results

The five reference simulations show that methane is predominantly withdrawn overhead, while the C_{3+} components are preferentially recovered in the bottoms. Table 1 presents the component recoveries R_i, defined as the component mass flow in the bottoms divided by its total mass flow in the overhead and bottoms products.

Recoveries for the 100 realistic feed compositions were estimated by local IDW interpolation in the coordinates C_3H_8, i-C_4H_{10}, n-C_4H_{10}, and C_{5+}. Application of the acceptance criteria yielded $F = 0.85$: 85 compositions were classified as PASS and 15 as FAIL.

The feasibility map shown in Fig. 2 uses the C_3H_8 mass fraction on the x-axis and the totali-C_4H_{10} + + n-C_4H_{10} fraction on the y-axis; marker size represents the C_{5+} fraction. A point is classified as PASS only when all component-recovery criteria are met. The boundary between PASS and FAIL therefore defines the estimated feed-composition limit for operation at the fixed set-points.

For transparency, the ranges across the 100 compositions are summarized in Table 2. They reflect the actual coverage of the set, showing that the sample is centered in the "working" corridor for C_3H_8, total C_4H_{10}, and C_{5+} fraction, with the sum of heavies kept within reasonable bounds.

Generation bounds were $C_3H_8 \in [0.06, 0.18]$, i-$C_4H_{10} \in [0.03, 0.12]$, n-$C_4H_{10} \in [0.03, 0.12]$, and $C_{5+} \in [0.02, 0.18]$, with $\Sigma(C_3H_8 + \text{i-}C_4H_{10} + \text{n-}C_4H_{10} + + C_{5+}) \in [0.15, 0.50]$. These limits cover the practical operating domain while excluding non-physical combinations.

Within the adopted acceptance criteria, propane recovery is the limiting factor: PASS/FAIL is most frequently triggered by the $R_{C_3H_8}$ constraint, whereas butanes and C_{5+} remain comparatively robust over the studied composition range. The region of stable operability

Table 1. Component recoveries for the reference cases (R_i = bottoms/(bottoms + overhead))

Case	R_{CH_4}	$R_{C_3H_8}$	$R_{\text{i-}C_4H_{10}}$	$R_{\text{n-}C_4H_{10}}$	$R_{C_{5+}}$
A — Lean	0.0054	0.9701	0.9930	0.9960	0.9988
B — Typical	0.0058	0.9042	0.9699	0.9814	0.9940
C — C_3-rich	0.0056	0.9014	0.9648	0.9775	0.9924
D — C_4-rich	0.0056	0.8849	0.9586	0.9735	0.9910
E — Heavies	0.0058	0.8478	0.9443	0.9639	0.9876

Table 2. Composition ranges for 100 realistic CH_4–C_{5+} feeds (mass fractions)

Metric	min	25th percentile	median	75th percentile	max	mean
C_3H_8	0.0600	0.0777	0.1005	0.1319	0.1800	0.1066
i-C_4H_{10}	0.0328	0.0474	0.0612	0.0781	0.1170	0.0648
n-C_4H_{10}	0.0310	0.0429	0.0626	0.0833	0.1191	0.0645
i-C_4H_{10} + n-C_4H_{10}	0.0643	0.1106	0.1265	0.1478	0.2307	0.1293
C_{5+}	0.0205	0.0441	0.0771	0.1030	0.1703	0.0767
$\Sigma(C_3H_8$ + i-C_4H_{10} + n-C_4H_{10} + $C_{5+})$	0.2197	0.2845	0.3076	0.3367	0.4389	0.3127
$CH_4 = 1 - \Sigma$(heavies)	0.5611	0.6633	0.6924	0.7155	0.7803	0.6873

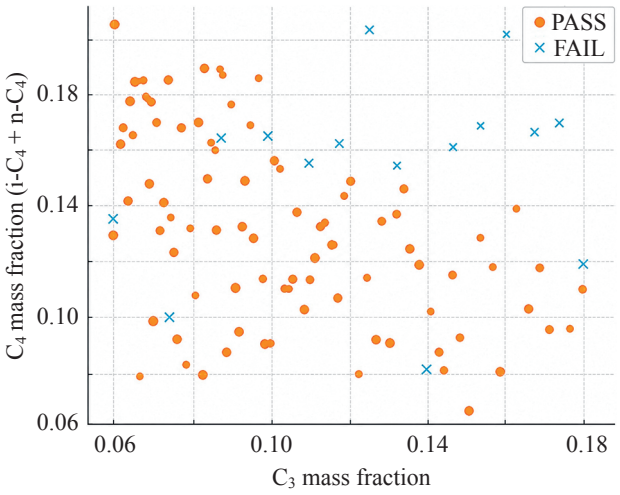

Fig. 2. PASS/FAIL map for 100 realistic feed compositions (marker size corresponds to the C_{5+} fraction)

occupies the central portion of the map; as C_3H_8 increases, the boundary descends already at moderate i-C_4H_{10} + + n-C_4H_{10} levels. A higher C_{5+} fraction nudges cases toward the boundary but rarely acts as the primary limiter. From an operating standpoint, this implies that — at fixed set-points — expanding the PASS region primarily calls for actions that improve propane retention (top temperature via the dephlegmator, effective liquid-to-vapor flow-rate ratio, and local heat-integration levers). To verify interpolation precisely where decisions hinge, we formed a short list of "borderline" feeds; their spot re-simulations at the same set-points serve as validation right at the decision boundary.

Discussion

The obtained PASS/FAIL map at fixed set-points and the share of admissible scenarios, $F = 0.85$ (85 out of 100), show that the LTR scheme in its current configuration remains operable for most typical feed-variability scenarios. The reference simulations set the scale: methane is predominantly rejected to the overhead product (the bottoms share is about 0.005–0.006), the heavy groups are recovered to the bottoms with a comfortable margin (for C_{5+} the recovery is around 0.99, for the butanes near 0.96–0.99). At the feasibility boundary the decisive variable is propane: its recovery ranges from about 0.97 on "light" feeds to about 0.85–0.90 on C_3/C_4-rich feeds, and it is propane that most often triggers failure. This conclusion is supported by the PASS/FAIL classification in the ($x_{C_3H_8}$, $x_{\text{i-}C_4H_{10}}$, $x_{\text{n-}C_4H_{10}}$) coordinates: failures occur predominantly when $R_{C_3H_8}$ falls below the threshold, while the recoveries of butanes and C_{5+} typically retain a comfortable margin. Physically, this reflects the role of the column top as a selective "filter": at the given pressures and dephlegmator temperature, butanes and C_{5+} condense more readily, whereas propane sits near the retention limit, so any increase in its feed fraction is quickly expressed as overhead loss.

The class split by composition corroborates this interpretation. Within PASS, the "typical" window is: C_3H_8 with a median of 0.097 (interquartile range 0.077–0.127), total C_4H_{10} with a median of 0.131 (0.104–0.157), and C_{5+} with a median of 0.071 (0.047–0.094). By contrast, in FAIL the medians are higher: C_3H_8 equals 0.132, total C_4H_{10} equals 0.163, C_{5+} equals 0.112, indicating a higher load on the dephlegmator and tighter cold requirements at the column top. The feasibility boundary is therefore anisotropic: sensitivity along the C_3H_8 axis is stronger than along total C_4H_{10}, and a heavier tail shifts the operating window downward in terms of allowable butanes at fixed propane.

From an operating standpoint, the position of this boundary is governed directly by conditions at the top of the column. Lowering the target temperature after the dephlegmator within hydraulic and thermal constraints increases propane return in the reflux and raises $R_{C_3H_8}$; a modest increase in the effective liquid-to-vapor flow-rate ratio has a similar effect and usually does not materially degrade the already high recoveries of the butanes and C_{5+}. The closer the current feed lies to the right on the C_3H_8 axis, the stronger the response to these levers, because the margin to the propane threshold is minimal there. Throughout such adjustments, it remains essential to preserve stable methane "throw" overhead, as this ensures the required quality of the top product; under the conditions considered, the CH_4 margin remains comfortable.

The scheme objective is to obtain at the bottoms a propane–butane mixture (Liquefied Petroleum Gas, LPG) with an admixture of heavier hydrocarbons for subsequent separation or use as fuel/feedstock. Within this configuration, ethane is predominantly a gas-phase component and is largely removed overhead together with methane; across the five references its contribution to the bottoms is small. Consequently, C_2H_6 is not included in the acceptance criteria: the PASS/FAIL classification and the final F are determined by the distributions of CH_4 and

the C_{3+} family. The overhead ethane-containing dry gas is technologically suitable as feed for further processing, including large-scale gas-processing/petrochemical complexes.

Finally, the scope of these conclusions should be outlined. All results pertain to the fixed set-points used in the problem statement; changing them would alter the unit "portrait" and the geometry of the PASS/FAIL region. The interpolation is valid within the composition domain coherently covered by the reference points; if new feed families appear (e.g., with a different i/n-C_4H_{10} ratio or a systematically different C_{5+} level), adding a targeted reference in the corresponding zone and updating the map avoids extrapolation. Within these bounds the unit exhibits high robustness: roughly eight to nine out of ten realistic scenarios meet the separation targets without retuning, and any further expansion of the PASS region is naturally linked to fine-tuning of top-end conditions via the dephlegmator set-point and control of the vapor–liquid ratio.

Conclusion

We propose and practically implement a compact procedure for assessing the operability of a Low-Temperature Rectification scheme at fixed set-points by transferring five reference simulations to a set of realistic Associated Petroleum Gas feeds. The key outputs are a PASS/FAIL map in the coordinates "mass fraction of C_3H_8 vs. total C_4H_{10} (i-C_4H_{10} + n-C_4H_{10})" and a single suitability metric *F*, which in the examined regime equals 0.85. This format shifts the problem from running dozens or hundreds of full simulations to quickly positioning any concrete feed relative to the operating window: given the mass fractions of C_3H_8, i-C_4H_{10}, n-C_4H_{10}, and C_{5+}, one can immediately see on which side of the boundary the unit will fall without retuning.

The approach is practically valuable in three ways. First, it reduces workload: instead of many model runs, it is sufficient to maintain a small reference set and classify new mixtures instantly. Second, it improves the predictability of control actions: the map makes clear how shifts along the C_3H_8 axis and the heavy tail move the boundary, allowing a prior estimate of whether adjustments at the column top are warranted. Third, it provides a common language for technologists, operators, and planning: the same operating window underpins feed acceptance, discussion of set-points, and medium-term planning of the LPG and dry-gas production.

The treatment of the light end follows the process objective. Ethane is not included in the acceptance criteria because, at the studied set-points, it predominantly leaves overhead with CH_4 and does not govern the C_{3+} separation target; it is shown in the reporting tables for mass-balance completeness and traceability, but it does not affect the classification or the value of operability index *F*. This is consistent with the target products of the unit: bottoms as a propane–butane mixture (LPG) with minor heavier hydrocarbons for downstream separation or fuel/feed use, and overhead as an ethane-containing dry gas suitable for further processing.

Deployment in plant practice is straightforward. At agreed intervals (e.g., seasonal shifts or a change of feed base), one can refresh one–two reference calculations in the new composition "zones" and recompute the map; this delivers controlled updating without inflating the simulation program. Integration requirements are minimal: inputs are routine — mass fractions of key groups and per-component "overhead/bottoms" splits at the references; outputs are a binary qualification and a readable two-dimensional map that can be stored alongside the feed registry and Key Performance Indicator reporting.

The method's limitations are transparent and define proper use. Conclusions hold for fixed set-points and within the composition domain coherently covered by the references; substantial changes to top pressure/temperature, addition of external refrigeration, or the emergence of new feed families (different i/n-butane ratio, systematically heavier tail) call for a local retuning by adding a targeted reference in the relevant zone. Within these bounds, the procedure yields a reproducible and operationally useful result: a fast, unambiguous decision on any real feed suitability, a clear view of sensitivity directions, and a practical lever for targeted adjustment of the regime — when, and only when, it is truly needed.

References

1. Bosman D.B., Li Q., Kiss A.A. Enhanced downstream processing of NGL using intensified fluid separation technologies. *Energy*, 2024, vol. 296, pp. 131186. doi: 10.1016/j.energy.2024.131186
2. Getu M., Mahadzir S., Long N.V.D., Lee M. Techno-economic analysis of potential natural gas liquid (NGL) recovery processes under variations of feed compositions. *Chemical Engineering Research and Design*, 2013, vol. 91, no. 7, pp. 1272–1283. doi: 10.1016/j.cherd.2013.01.015
3. Qyyum M.A., Naquash A., Haider J., Al-Sobhi S.A., Lee M. State-of-the-art assessment of natural gas liquids recovery processes: Techno-economic evaluation, policy implications, open issues, and the way forward. *Energy*, 2022, vol. 238, part A, pp. 121684. doi: 10.1016/j.energy.2021.12168.
4. Li Y., Xu F., Gong C. System optimization of turbo-expander process for natural gas liquid recovery. *Chemical Engineering Research and Design*, 2017, vol. 124, pp. 159–169. doi: 10.1016/j.cherd.2017.06.001
5. Hajizadeh A., Mohamadi-Baghmolaei M., Azin R., Osfouri S., Heydari I. Technical and economic evaluation of flare gas recovery in a giant

Литература

1. Bosman D.B., Li Q., Kiss A.A. Enhanced downstream processing of NGL using intensified fluid separation technologies // Energy. 2024. V. 296. P. 131186. doi: 10.1016/j.energy.2024.131186
2. Getu M., Mahadzir S., Long N.V.D., Lee M. Techno-economic analysis of potential natural gas liquid (NGL) recovery processes under variations of feed compositions // Chemical Engineering Research and Design. 2013. V. 91. N 7. P. 1272–1283. doi: 10.1016/j.cherd.2013.01.015
3. Qyyum M.A., Naquash A., Haider J., Al-Sobhi S.A., Lee M. State-of-the-art assessment of natural gas liquids recovery processes: Techno-economic evaluation, policy implications, open issues, and the way forward // Energy. 2022. V. 238. Part A. P. 121684. doi: 10.1016/j.energy.2021.121684
4. Li Y., Xu F., Gong C. System optimization of turbo-expander process for natural gas liquid recovery // Chemical Engineering Research and Design. 2017. V. 124. P. 159–169. doi: 10.1016/j.cherd.2017.06.001
5. Hajizadeh A., Mohamadi-Baghmolaei M., Azin R., Osfouri S., Heydari I. Technical and economic evaluation of flare gas recovery in

gas refinery. *Chemical Engineering Research and Design*, 2018, vol. 131, pp. 506–519. doi: 10.1016/j.cherd.2017.11.026
6. Nezhadfard M., Khalili-Garakani A. Power generation as a useful option for flare gas recovery: Enviro-economic evaluation of different scenarios. *Energy*, 2020, vol. 204, pp. 117940. doi: 10.1016/j.energy.2020.117940
7. Eshaghi S., Hamrang A. An innovative techno-economic analysis for the selection of an integrated ejector system in the flare gas recovery of a refinery plant. *Energy*, 2021, vol. 228, pp. 120594. doi: 10.1016/j.energy.2021.120594
8. Rahimpour M.R., Jamshidnejad Z., Jokar S.M., Karimi G., Ghorbani A., Mohammadi A.H. A comparative study of three different methods for flare gas recovery of Asalooye Gas Refinery. *Journal of Natural Gas Science and Engineering*, 2012, vol. 4, pp. 17–28. doi: 10.1016/j.jngse.2011.10.001
9. Tahouni N., Gholami M., Panjeshahi M.H. Integration of flare gas with fuel gas network in refineries. *Energy*, 2016, vol. 111, pp. 82–91. doi: 10.1016/j.energy.2016.05.055
10. Khanipour M., Mirvakili A., Bakhtyari A., Farniaei M., Rahimpour M.R. Enhancement of synthesis gas and methanol production by flare gas recovery utilizing a membrane based separation process. *Fuel Processing Technology*, 2017, vol. 166, pp. 186–201. doi: 10.1016/j.fuproc.2017.06.008
11. Soltanieh M., Zohrabian A., Gholipour M.J., Kalnay E. A review of global gas flaring and venting and impact on the environment: Case study of Iran. *International Journal of Greenhouse Gas Control*, 2016, vol. 49, pp. 488–509. doi: 10.1016/j.ijggc.2016.02.010
12. Fawole O.G., Cai X.-M., MacKenzie A.R. Gas flaring and resultant air pollution: A review focusing on black carbon. *Environmental Pollution*, 2016, vol. 216, pp. 182–197. doi: 10.1016/j.envpol.2016.05.075
13. Faramawy S., Zaki T., Sakr A.A.-E. Natural gas origin, composition, and processing: A review. *Journal of Natural Gas Science and Engineering*, 2016, vol. 34, pp. 34–54. doi: 10.1016/j.jngse.2016.06.030
14. Mokhatab S., Poe W.A. *Handbook of Natural Gas Transmission and Processing: Principles and Practices*. Gulf Professional Publishing, 2012, 828 p.
15. Speight J.G. *Natural Gas: A Basic Handbook*. Gulf Professional Publishing, 2018, 462 p.
16. *GPSA Engineering Data Book*. Gas Processors Suppliers Association, 2004, 820 p.
17. Ekwonu M.C., Perry S., Oyedoh E.A. Modelling and simulation of gas engines using Aspen HYSYS. *Journal of Engineering Science and Technology Review*, 2013, vol. 6, pp. 1–4.
18. Roy P.S., Amin M.R. Aspen-HYSYS simulation of natural gas processing plant. *Journal of Chemical Engineering*, 2011, vol. 26, no. 1, pp. 62–65. doi: 10.3329/jce.v26i1.10186

a giant gas refinery // Chemical Engineering Research and Design. 2018. V. 131. P. 506–519. doi: 10.1016/j.cherd.2017.11.026
6. Nezhadfard M., Khalili-Garakani A. Power generation as a useful option for flare gas recovery: Enviro-economic evaluation of different scenarios // Energy. 2020. V. 204. P. 117940. doi: 10.1016/j.energy.2020.117940
7. Eshaghi S., Hamrang A. An innovative techno-economic analysis for the selection of an integrated ejector system in the flare gas recovery of a refinery plant // Energy. 2021. V. 228. P. 120594. doi: 10.1016/j.energy.2021.120594
8. Rahimpour M.R., Jamshidnejad Z., Jokar S.M., Karimi G., Ghorbani A., Mohammadi A.H. A comparative study of three different methods for flare gas recovery of Asalooye Gas Refinery // Journal of Natural Gas Science and Engineering. 2012. V. 4. P. 17–28. doi: 10.1016/j.jngse.2011.10.001
9. Tahouni N., Gholami M., Panjeshahi M.H. Integration of flare gas with fuel gas network in refineries // Energy. 2016. V. 111. P. 82–91. doi: 10.1016/j.energy.2016.05.055
10. Khanipour M., Mirvakili A., Bakhtyari A., Farniaei M., Rahimpour M.R. Enhancement of synthesis gas and methanol production by flare gas recovery utilizing a membrane based separation process // Fuel Processing Technology. 2017. V. 166. P. 186–201. doi: 10.1016/j.fuproc.2017.06.008
11. Soltanieh M., Zohrabian A., Gholipour M.J., Kalnay E. A review of global gas flaring and venting and impact on the environment: Case study of Iran // International Journal of Greenhouse Gas Control. 2016. V. 49. P. 488–509. doi: 10.1016/j.ijggc.2016.02.010
12. Fawole O.G., Cai X.-M., MacKenzie A.R. Gas flaring and resultant air pollution: A review focusing on black carbon // Environmental Pollution. 2016. V. 216. P. 182–197. doi: 10.1016/j.envpol.2016.05.075
13. Faramawy S., Zaki T., Sakr A.A.-E. Natural gas origin, composition, and processing: A review // Journal of Natural Gas Science and Engineering. 2016. V. 34. P. 34–54. doi: 10.1016/j.jngse.2016.06.030
14. Mokhatab S., Poe W.A. Handbook of Natural Gas Transmission and Processing: Principles and Practices. Gulf Professional Publishing, 2012. 828 p.
15. Speight J.G. Natural Gas: A Basic Handbook. Gulf Professional Publishing, 2018. 462 p.
16. GPSA Engineering Data Book. Gas Processors Suppliers Association, 2004. 820 p.
17. Ekwonu M.C., Perry S., Oyedoh E.A. Modelling and simulation of gas engines using Aspen HYSYS // Journal of Engineering Science and Technology Review. 2013. V. 6. P. 1–4.
18. Roy P.S., Amin M.R. Aspen-HYSYS simulation of natural gas processing plant // Journal of Chemical Engineering. 2011. V. 26. N 1. P. 62–65. doi: 10.3329/jce.v26i1.10186

Authors

Vadim O. Kholyavkin — PhD Student, ITMO University, Saint Petersburg, 197101, Russian Federation, https://orcid.org/0009-0006-3263-822X, vadimixl@itmo.ru
Ekaterina V. Logvinenko — PhD, Associate Professor, ITMO University, Saint Petersburg, 197101, Russian Federation, https://orcid.org/0000-0002-2155-2109, evlogvinenko@itmo.ru

Авторы

Холявкин Вадим Олегович — аспирант, Университет ИТМО, Санкт-Петербург, 197101, Российская Федерация, https://orcid.org/0009-0006-3263-822X, vadimixl@itmo.ru
Логвиненко Екатерина Владимировна — кандидат технических наук, доцент, Университет ИТМО, Санкт-Петербург, 197101, Российская Федерация, https://orcid.org/0000-0002-2155-2109, evlogvinenko@itmo.ru

Received 19.01.2026
Approved after reviewing 10.08.2026
Accepted 20.09.2026

Статья поступила в редакцию 19.01.2026
Одобрена после рецензирования 10.08.2026
Принята к печати 20.09.2026

Работа доступна по лицензии
Creative Commons
«Attribution-NonCommercial»